Chemical Data Collections 52 (2024) 101155

Contents lists available at ScienceDirect

Chemical Data Collections

journal homepage: www.elsevier.com/locate/cdc

Data Article

High-throughput thiophene adsorption calculations on bimetallic surfaces

Soleil Chapman, Innis Michael, Walter Malone *

Department of Physics, Tuskegee University, 1200W. Montgomery Rd., Tuskegee, AL 36088, United States

ARTICLE INFO

Keywords:
DFT
Thiophene
Bimetallic surfaces
Adsorption

ABSTRACT

We present a high-throughput screening of thiophene (SC_4H_s) on bimetallic (100) surfaces in select adsorption sites. We present the adsorption energies, charge transfer to the S atom, and C-S bond lengths on each of the surfaces studied. We note that thiophene remains intact over the majority of the bimetallic surfaces, only breaking C-S bonds over 33 of the 1131 different surfaces studied. Overall, we note a positive correlation between charge transfer to the S atom and C-S bond lengths. We also report that many of the surfaces experience a large buckling of the first layer of the surface. We have made this dataset publicly available in the hopes that it will aid the search for novel hydrodesulfurization catalysts and aid the progress of employing machine learning in chemistry.

Specifications Table

Subject area	*Computational Chemistry*
Compounds	*Thiophene (SC_4H_4)*
Data category	*computational simulations*
Data acquisition format	*geometry optimizations, Bader charge analysis*
Data type	*Raw, analyzed, simulated,*
Procedure	*Density functional theory geometry calculations using the BEEF-vdW functional of thiophene adsorbed on various bimetallic (100) surfaces. Charge transfer to the thiophene molecules was preformed using the Bader charge analysis*
Data accessibility	*Raw data is available on the Materials Cloud Archive.* *ID#: materialscloud:2023.169* *URL:* https://archive.materialscloud.org/record/2023.169

1. Rationale

The emission of sulfur oxide pollutants through the burning of chemical fuels contributes to acid rain and smog [1]. As such, government agencies continually lower the maximum allowable sulfur content in fuels. To meet the demand for fuels with lower sulfur

* Corresponding author.
E-mail address: wmalone@tuskegee.edu (W. Malone).

https://doi.org/10.1016/j.cdc.2024.101155
Received 6 April 2024; Received in revised form 3 June 2024; Accepted 3 July 2024
Available online 4 July 2024

content, it becomes important to design novel, more efficient hydrodesulfurization (HDS) catalysts. HDS [2], the process by which organosulfur compounds are removed from petrochemicals, is poorly understood, though, for some of the simplest molecules targeted for desulfurization, impeding the discovery of novel HDS catalysts. Thiophene (C_4H_4S), one such simple molecule, is both difficult to desulfurize, due to the stability of its aromatic ring [3–5], and the process by which desulfurization occurs is still debated.

To study the thiophene HDS catalyst problem, many have opted to model the active sites of more complex catalysts with single crystal metal surfaces [6–14]. Many of these computational studies revealed important information about the thiophene HDS process [5,15–36]. For instance, a report by Zhu et al. found thiophene can proceed along the direct desulfurization pathway on Ni(111) and Ni_{55} nanoclusters [37], while Mittendorfer et al. found hydrogenation can reduce the energy barrier for desulfurization [38]. Moreover, the propensity of thiophene to spontaneously break a C-S bond has been noted over many transition metal surfaces such as Ni [38–41], Mo, W, Cr, V, Nb, and Ta(100) [42] surfaces. Some catalyst built from these metals, though, have low HDS rates due to the thiol fragment binding very strongly to the surface, poisoning the catalyst [43].

Adsorption energy, or how strongly the molecule binds to the surface, is just one of many chemical descriptors [43–46] that often are mapped to catalytic activity. Other examples of these descriptors include charge transfer, d-band properties of the surface, and electronegativity of the atoms in the surface. While small theoretical studies have proven useful, recent advances in machine learning have made screening large portions of chemical space possible, greatly increasing the possibility of discovering novel catalysts [47–50]. To effectively utilize machine learning, one needs a large database of high-level theoretical calculations or experimental data. To date, high-throughput screening attempts have led to the creation of various large databases [51–54] with some containing systems of atoms or small molecules adsorbed on bimetallic surfaces usually using Density Functional Theory (DFT), a computational method that provides a good balance between computational accuracy and computational cost [55]. DFT has seen many successes predicting material properties, yet even its reasonable computational speed has made creating large datasets challenging for machine learning applications. As such, a large dataset of thiophene calculations is still missing, severely impeding the process of discovering novel HDS catalysts.

To remedy this problem, we present a substantial, publicly available, database of DFT thiophene adsorption calculations on various (100) transition metal surfaces. We choose the (100) surface as the adsorption properties on this facet have been shown to correlate well with HDS activity on more complex transition-metal-sulfides [43]. The remainder of this report is laid out as follows: in Section 2 we discuss the procedure, in Section 3 we present a brief discussion of the data, and in Section 4 we present our conclusions.

2. Procedure

Geometry optimization was carried out with the Quantum Espresso first-principle electronic-structure software suite [56,57] with a

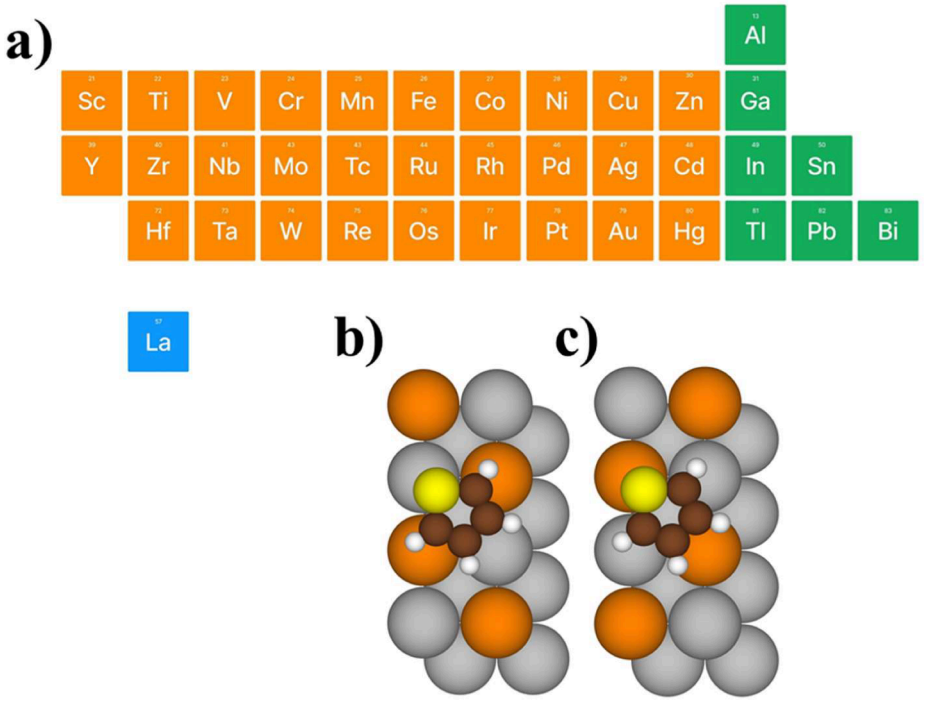

Fig. 1. a) Illustration of all elements used to build the bimetallic surfaces A_3B, b) hollow-45-a adsorption site, and c) hollow-45-b adsorption site. Yellow atoms represent S atoms, brown atoms represent C atoms, white atoms represent H atoms, orange atoms represent A atoms, and silver atoms represent B atoms.

0.026 eV/Å force criterion and 0.15 eV Fermi smearing. Each surface was modeled using a 2 × 4 atom four-layer slab. To make the study more computationally feasible, the 2 × 4 unit cell was chosen as it was the smallest unit cell in which a thiophene molecule could be placed horizontally on the surface. We anticipate there may be some molecule-molecule interactions at this coverage. However, some molecule-molecule interactions are closer to HDS reaction conditions which occur at high pressures. The plane-wave cutoff was set at 490 eV while the Brillouin zone was sampled using a Monkhorst-Pack 6 × 3 × 1 k-point mesh. For the DFT functional, we employed the BEEF-vdW functional [58], which operates at the level of the generalized gradient approximation [59–61]; that is total energy is a function of the charge density and the gradient of the charge density. BEEF-vdW also contains a nonlocal contribution to the total energy to account for the van der Waals interaction, which is important for the description of many systems including the adsorption of small molecules, such as thiophene, on transition metal surfaces [17,62–68].

Continuing forward, we calculated adsorption energy, E_{ads}, as:

$$E_{ads} = -E_{thio/sub} + E_{sub} + E_{thio} \quad (1)$$

Where E_{thio} is the total energy of the thiophene molecule in the gas phase, E_{sub} is the total energy of the clean relaxed substrate, and $E_{thio/sub}$ is the total energy of the thiophene molecule relaxed on the substrate. With this definition the more positive an adsorption energy the stronger the thiophene molecule binds to the surface. In addition to adsorption energy, we also computed charge transfer from the surface to both the thiophene molecule and the S atom using the Bader charge analysis [69–72].

As mentioned, our surfaces were constructed using four-layer slabs. As Quantum Espresso uses periodic boundary conditions, at least 15 Å of vacuum was used to separate neighboring slabs. The coordinates of the bottom three layers were fixed while the top layer and the thiophene molecule were allowed to relax. The lattice constants for each alloy was taken from a similar high-throughput study [73] that also utilized the BEEF-vdW functional. For Fe, Ni, Co, and Mn spin-polarized calculations were performed with a starting magnetic moment of 3, 3, 2, and 1 μ_b respectively. These initial values were also taken from the same study [73]. Fig. 1a) illustrates the metals involved in the study. From these 37 elements, $L1_2$ alloys, chemical formula A_3B, were created and then cleaved to create (100) surface slabs. This leads to slabs that repeat over two layers with one layer of all A atoms and the second layer with 50 % A atoms and 50 % B atoms. For our database, given our limited computational resources we chose to study surfaces terminated with the 50 %/50 % A:B layer as we anticipated those surfaces would be more interesting; that is second layer atom effects will be less prominent than first layer atom effects on thiophene adsorption, meaning the surfaces terminated with the 100 % A atom layer would yield thiophene adsorption properties more similar to single metal surfaces. Fig. 1b) and c) illustrates a general outlook of the (100) surface and the two adsorption sites that were chosen to build our dataset. These two hollow sites, we call hollow-45-a and hollow-45-b, were chosen as this site, on single metal (100) surfaces, has been demonstrated to consistently give the largest adsorption energies for intact thiophene [17,20,39,42]. As the study in reference 72 also built bimetallic surfaces we only studied surfaces they found to converge; that is alloys free from electronic structure convergence issues or a mismatch in magnetic structure in either the clean surface or the surface/-thiophene system. Taking reference 72 as a baseline for what surfaces would converge, we still found a few surfaces, as expected, that had convergence problems as (111) surfaces, what reference 72 studied, are generally more stable than (100) surfaces. Altogether, we successfully relaxed thiophene over 1131 different surfaces resulting in 2235 completed calculations.

3. Data, value and validation

All output files were uploaded to the Materials Cloud Archive. A permanent link to the data is found at the beginning of this manuscript. Despite hollow-45 keeping thiophene intact on all single element surfaces [42], on bimetallic surfaces this site still manage to break in a small number of cases. Specifically, thiophene broke at least one C-S bond on 33 different surfaces. This is a relatively

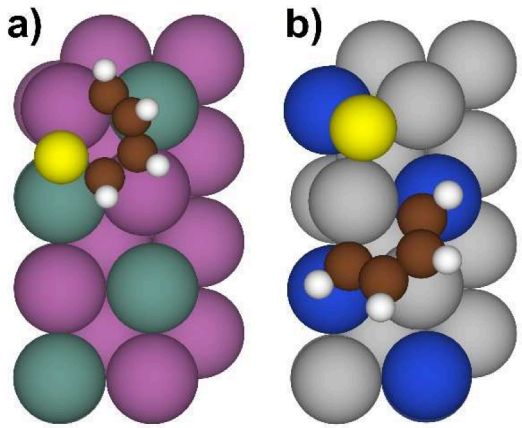

Fig. 2. Most common adsorption configurations with a) one broken C-S bond and b) two broken C-S bonds. Yellow atoms represent S atoms, brown atoms represent C atoms, white atoms represent H atoms, purple atoms *Sc* atoms, dark green atoms represent Y atoms, silver atoms represent Hf atoms, and blue atoms represent Cu atoms.

small fraction of our entire dataset, less than 1.5 % of all configurations. Moreover, these surfaces are unlikely to be optimal for HDS as the strong interaction needed to break thiophene completely apart can lead to catalyst poisoning. In our previous study, we found a negative correlation between HDS rate and metals that broke thiophene [43]. However, for completeness we will briefly discuss these configurations. Fig. 2a) illustrates the most common resulting configuration when thiophene broke one C-S bond. Fig. 2a) specifically illustrates adsorption on Y_3Sc. However, very similar configurations resulted on many of the surfaces that broke thiophene. In this configuration, the S atom and C atom, with the broken C-S bond, bond to a metal atom. Another alternate configuration with one broken C-S bond, occurring on Mo_3La, resulted in only one side of the molecular fragment bonded to the surface. For surfaces that broke two C-S bonds, Fig. 2b) illustrates the resulting configuration. Fig. 2b) specifically illustrates adsorption on Hf_3Cu. However, again very similar configurations resulted on many of the surfaces that broke thiophene. In this configuration the S atom and the separated molecular fragment bond to different points on the surface. The S atom, when it breaks off thiophene, appears to have no strong preference for where it eventually binds to the surface. In Fig. 2b), we see the S atom bond slightly off center to a hollow site, giving the atom a threefold coordination with the surface. The S atom could also sit directly on a hollow site or atop a single surface atom. One different alternate configuration occurred on Re_3Pb, where the molecular fragment further decomposed into a pair of C_2H_2 molecules. Continuing, when thiophene breaks at least one C-S bond it allows the S atom to form new bonds with the metal atoms in the surface, weakening the metal-metal bonds. To analyze this, we computed the average change in the metal-metal bonds in the first layer of the surface. For configurations where thiophene broke we noted a 6.6 % increase in the length of these bonds after relaxation while

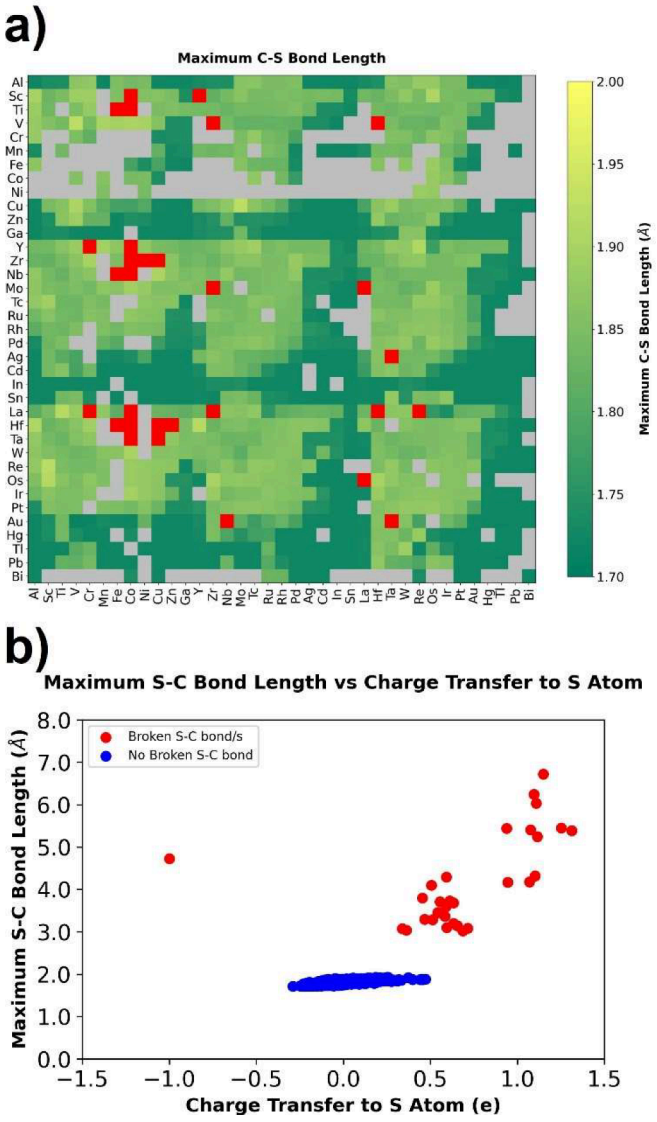

Fig. 3. a) Maximum C-S bond length for thiophene adsorbed on bimetallic surfaces. Gey boxes represent surfaces for which the thiophene calculation did not converge. The y-axis denotes the A_3 element while the x-axis denotes the B element. b) Maximum S-C bond length vs charge transfer to the S atom.

for the remainder of the configurations, where thiophene remained intact, we noted on average only a 2.9 % increase in these bond lengths. Taken together, these results demonstrate that some of these surfaces are active enough to break apart thiophene in hollow-45, which generally leaves the molecule intact.

To further examine the resulting adsorption configurations, in Fig. 3a) we plot the maximum C-S bond length for the highest adsorption energy configuration on each surface. From Fig. 3a) we see a clear distinction between configurations with and those without a broken C-S bond. Intact configurations maintain C-S distances less than 2.00 Å. In contrast, those configurations, denoted by red boxes in Fig. 3a), with broken C-S bonds had maximum C-S distances over 2.8 Å, demonstrating a clear distinction between the two adsorption scenarios. Among those intact configurations, which occurred on the vast majority of surfaces, we noted a wide range of bond lengths from 1.70 Å to just under 2.00 Å. Unsurprisingly, we noticed alloys with elements on the right of the periodic table, with fuller d-orbitals, tended to result in smaller C-S bond lengths, indicating a weaker interaction of thiophene with the surface. Fig. 3a) also conveniently illustrates which metals failed to converge with grey squares. These surfaces, as mentioned, faced electronic structure convergence issues, or were previously shown to have these issues [73]. These surfaces commonly contained Ni, Fe, Co, and Mn, our magnetic elements, as the element that composed 75 % of the surface, or Bi as any element in the surface, indicating that DFT has difficulty modeling these elements. Common reasons for divergence include the well-known "charge-sloshing problem" [74–77], where a small enough HOMO-LUMO gap can lead to an oscillation of orbital shapes. As one knows, a small HOMO-LUMO gap leads to a high polarizability. If the polarizability is high enough even a small error in the Kohm Sham potential may lead to a large oscillation of the electron density, causing the self-consistent field (scf) routine to fail to converge. Furthermore, If the HOMO-LUMO gap is small enough the order of orbitals may change such that a previously unoccupied orbital becomes occupied and a previously occupied orbital becomes unoccupied [77,78]. This will, of course, cause a large change in the density matrix such that the electron density, from the previous scf step, no longer becomes a good guess for the next scf step, preventing convergence as these two closely spaced orbitals continually switch from being occupied to unoccupied. It is likely one of these reasons that contributed to the limited number of systems where the scf cycle failed to converge.

To further explore the adsorption geometry, we plot in Fig. 3b) the maximum C-S bond length vs the charge transfer to the S atom. In the gas phase, thiophene's C-S bond length is calculated to be 1.72 Å. These two quantities, in previous studies, have been demonstrated to be correlated [42]. Indeed, as demonstrated by Fig. 3b), on bimetallic surfaces this correlation exists too. For intact thiophene adsorption configurations, blue dots in Fig. 3b), we note a general positive correlation between charge transferred to the S atom and maximum C-S bond length. As the charge to the S atom increases so does the maximum C-S bond length, suggesting this excess charge serves to weaken the C-S bonds of the thiophene molecule. When thiophene breaks apart, denoted by red dots in Fig. 3a), the correlation also exists but is now much steeper. This occurs as after the S atom acquires enough charge and breaks two C-S bonds, the C-S distances rapidly increase due to the S atom settling in a different part of the surface compared to the remaining molecular fragment. Overall, we note that the S atom takes charge when thiophene breaks bonds. The one exception to this rule is Mo_3La, where thiophene breaks a single C-S bond but the S atom gives charge away. This also happens to be the configuration where only one end of the molecular fragment bonds to the Mo_3La surface.

Moving further, we also examined the adsorption energy and charge transfer to the S atom for the highest adsorption energy configuration on each surface. Fig. 4a) illustrates the adsorption energy for the highest adsorption energy configuration for each surface. Grey boxes are again surfaces that possessed convergence issues. Overall, we note an average adsorption energy of 1.69 eV with a few high adsorption energy outliers. These outliers, usually, exist because thiophene in those configurations leads to a large vertical buckling of the surface. The relatively large displacement of atoms in the z-direction can lead to a large difference in the total energy of the clean relaxed surface and the relaxed surface after adsorption. We see a variety of these surfaces when Ag or Au composes 75 % of the slab or X_3Re surfaces. A large buckling often suggests these surfaces may be metastable or unstable, preferring to

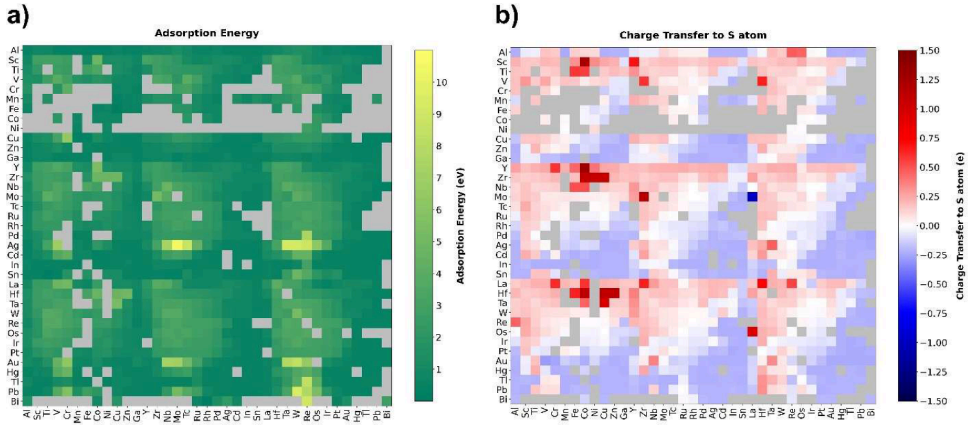

Fig. 4. a) Adsorption energy for thiophene adsorbed on bimetallic surfaces, and c) Charge Transfer to the S atom for thiophene adsorbed on bimetallic surfaces. Gey boxes represent surfaces for which thiophene calculation did not converge. The y-axis denotes the A3 element while the x-axis denotes the B element.

reconstruct. We also briefly explored the effects of coverage on adsorption energy, to better understand the adsorption process, by picking five random alloys and performing geometric relaxations on both adsorption sites in a 4 × 4 unit cell, effectively halving the coverage. The results are printed in table S1in the supplementary information. We note, as expected, decreasing coverage notably changes the adsorption energy. However, as previously stated we believe the higher coverage is closer to what experimental HDS reaction conditions are. To summarize the results, the adsorption energy changed, for most configurations, by 10 % or less. Some configurations experienced a fair bit more change in the adsorption energy, indicating the substrate mediated molecule-molecule interactions are highly dependent on the alloy. They also may play an important role in the breaking of thiophene. Two configurations for which thiophene broke in the 2 × 4 unit cell, remained intact in the larger 4 × 4 unit cell.

Moving further, Fig. 4b) illustrates the charge transfer to the S atom for the highest adsorption energy configuration on each surface. Grey boxes are again the surfaces with convergence issues. From Fig. 4b), we note that on most surfaces S charge transfer is small; between 0.5 e and −0.5 e. The average charge transfer was 0.0 e and, indeed, on a good number of surfaces the charge transfer was, in fact, 0.0 e, denoted by white boxes in Fig. 4b). We also note from Fig. 4b) that surfaces with charge transfer to the S atom, denoted by dark red and dark blue squares, usually contain Y, Zr, Nb, Mo, *Sc*, Ti, La, Ta, Co, Zn, or Cu. Overall, we note that charge transfer as well as adsorption energy is highly dependent on the surface.

4. Conclusions

We have presented a large dataset of thiophene adsorption calculations on (100) bimetallic surfaces. We report a large range of adsorption energies and charge transfer to the S atom. We note that charge transfer and S-C bond lengths tend to be correlated with the larger C-S bond lengths being associated with more charge transfer to the S atom. Unlike previous theoretical studies on single element surfaces, we calculate thiophene to break C-S bonds on a small number of bimetallic surfaces. On these surfaces, charge transfer to the S atom tends to be the greatest.

We hope this dataset will advance the discovery of novel HDS catalysts and other reactions that may involve thiophene. We also hope this dataset will aid the community that utilizes machine learning in physics, chemistry, and material science by providing a needed training dataset of a larger adsorbate. As data-driven machine learning methods become more prominent, larger datasets to train models will continually become more important.

CRediT authorship contribution statement

Soleil Chapman: Writing – review & editing, Visualization, Investigation, Formal analysis. **Innis Michael:** Writing – review & editing, Investigation, Formal analysis. **Walter Malone:** Writing – review & editing, Writing – original draft, Visualization, Supervision, Methodology, Investigation, Formal analysis, Data curation, Conceptualization.

Declaration of competing interest

The authors declare that they have no known competing financial interests or personal relationships that could have appeared to influence the work reported in this paper.

Data availability

Data will be made available on request.

Acknowledgements

This work was supported by the donors of ACS Petroleum Research Fund under Undergraduate New Investigator Grant 65980-UNI5. Walter Malone served as Principal Investigator on ACS PRF 65980-UNI5 that provided support for Soleil Chapman and Innis Michael.

Walter Malone acknowledges support from National Science Foundation RISE grant #2122985.

This work used Avil at Purdue University through allocation PHY220147 from the Advanced Cyberinfrastructure Coordination Ecosystem: Services & Support (ACCESS) program [79], which is supported by National Science Foundation grants #2138259, #2138286, #2138307, #2137603, and #2138296.

Supplementary materials

Supplementary material associated with this article can be found, in the online version, at doi:10.1016/j.cdc.2024.101155.

References

[1] D. Duayne Whitehurst, T. Isoda, I. Mochida, Present state of the art and future challenges in the hydrodesulfurization of polyaromatic sulfur compounds. Advances in Catalysis, Elsevier, 1998, pp. 345–471, https://doi.org/10.1016/S0360-0564(08)60631-8.

[2] A. Tanimu, K. Alhooshani, Advanced hydrodesulfurization catalysts: a review of design and synthesis, Energy Fuels. 33 (2019) 2810–2838, https://doi.org/10.1021/acs.energyfuels.9b00354.

[3] S. Terada, T. Yokoyama, M. Sakano, A. Imanishi, Y. Kitajima, M. Kiguchi, Y. Okamoto, T. Ohta, Thiophene adsorption on Pd(111) and Pd(100) surfaces studied by total-reflection S K-edge X-ray absorption fine-structure spectroscopy, Surf. Sci. 414 (1998) 107–117, https://doi.org/10.1016/S0039-6028(98)00495-6.

[4] B.C. Wiegand, C.M. Friend, Model studies of the desulfurization reactions on metal surfaces and in organometallic complexes, Chem. Rev. 92 (1992) 491–504, https://doi.org/10.1021/cr00012a001.

[5] H. Wang, E. Iglesia, Thiophene hydrodesulfurization catalysis on supported Ru clusters: mechanism and site requirements for hydrogenation and desulfurization pathways, J. Catal. 273 (2010) 245–256, https://doi.org/10.1016/j.jcat.2010.05.019.

[6] P. Moses, B. Hinnemann, H. Topsoe, J. Norskov, The hydrogenation and direct desulfurization reaction pathway in thiophene hydrodesulfurization over MoS2 catalysts at realistic conditions: a density functional study, J. Catal. 248 (2007) 188–203, https://doi.org/10.1016/j.jcat.2007.02.028.

[7] A.J. Gellman, M.H. Farias, M. Salmeron, G.A. Somorjai, A thermal desorption study of thiophene adsorbed on the clean and sulfided Mo(100) crystal face, Surf. Sci. 136 (1984) 217–228, https://doi.org/10.1016/0039-6028(84)90666-6.

[8] A. Gellman, The catalytic hydrodesulfurization of thiophene on the Mo(100) crystal surface, J. Catal. 88 (1984) 546–548, https://doi.org/10.1016/0021-9517(84)90039-3.

[9] M. Bussell, A radiotracer (14C) and catalytic study of thiophene hydrodesulfurization on the clean and carbided Mo(100) single-crystal surface, J. Catal. 106 (1987) 93–104, https://doi.org/10.1016/0021-9517(87)90214-4.

[10] M.E. Bussel, A.J. Gellman, G.A. Somorjai, The role of adsorbate overlayers in thiophene hydrodesulfurization over molybdenum and rhenium single crystals, Catal Lett 1 (1988) 195–201, https://doi.org/10.1007/BF00766174.

[11] M. Bussell, Thiophene hydrodesulfurization over transition metal surfaces: structure insensitive over molybdenum and structure sensitive over rhenium, J. Catal. 110 (1988) 423–426, https://doi.org/10.1016/0021-9517(88)90336-3.

[12] D.G. Kelly, M. Salmeron, G.A. Somorjai, The adsorption and reactions of hydrocarbons on Molybdenum single crystal surfaces; when clean and in the presence of co-adsorbed sulfur or carbon, Surf. Sci. 175 (1986) 465–486, https://doi.org/10.1016/0039-6028(86)90007-5.

[13] A. Gellman, Catalytic hydrodesulfurization over the Mo(100) single crystal surface I. Kinetics and overall mechanism, J. Catal. 107 (1987) 92–102, https://doi.org/10.1016/0021-9517(87)90275-2.

[14] A.J. Gellman, M.E. Bussell, G.A. Somorjai, Catalytic hydrodesulfurization over the Mo(100) single crystal surface, J. Catal. 107 (1987) 103–113, https://doi.org/10.1016/0021-9517(87)90276-4.

[15] F. Mittendorfer, J. Hafner, A DFT study of the adsorption of thiophene on Ni(100), Surf. Sci. 492 (2001) 27–33, https://doi.org/10.1016/S0039-6028(01)01424-8.

[16] S.J. Jenkins, Aromatic adsorption on metals via first-principles density functional theory, Proc. R. Soc. A. 465 (2009) 2949–2976, https://doi.org/10.1098/rspa.2009.0119.

[17] W. Malone, J. Matos, A. Kara, Adsorption of thiophene on transition metal surfaces with the inclusion of van der Waals effects, Surf. Sci. 669 (2018) 121–129, https://doi.org/10.1016/j.susc.2017.11.013.

[18] P. Sony, P. Puschnig, D. Nabok, C. Ambrosch-Draxl, Importance of Van Der Waals interaction for organic molecule-metal junctions: adsorption of thiophene on Cu(110) as a prototype, Phys. Rev. Lett. 99 (2007) 176401, https://doi.org/10.1103/PhysRevLett.99.176401.

[19] C. Morin, A. Eichler, R. Hirschl, P. Sautet, J. Hafner, DFT study of adsorption and dissociation of thiophene molecules on Ni(110), Surf. Sci. 540 (2003) 474–490, https://doi.org/10.1016/S0039-6028(03)00888-4.

[20] H. Orita, N. Itoh, Adsorption of thiophene on Ni(100), Cu(100), and Pd(100) surfaces: ab initio periodic density functional study, Surf. Sci. 550 (2004) 177–184, https://doi.org/10.1016/j.susc.2003.12.014.

[21] R. Duschek, F. Mittendorfer, R.I.R. Blyth, F.P. Netzer, J. Hafner, M.G. Ramsey, The adsorption of aromatics on sp-metals: benzene on Al(111), Chem. Phys. Lett. 318 (2000) 43–48, https://doi.org/10.1016/S0009-2614(99)01457-8.

[22] R.I.R. Blyth, F. Mittendorfer, J. Hafner, S.A. Sardar, R. Duschek, F.P. Netzer, M.G. Ramsey, An experimental and theoretical investigation of the thiophene/aluminum interface, J. Chem. Phys. 114 (2001) 935–942, https://doi.org/10.1063/1.1332080.

[23] A. Benbella, H. Jabraoui, I. Matrane, M. Mazroui, Exploring adsorption behavior of sulfur and nitrogen compounds on transition metal-doped Cu(100) surfaces: insights from DFT and MD simulations, Phys. Chem. Chem. Phys. 25 (2023) 27553–27565, https://doi.org/10.1039/D3CP04379G.

[24] S.M. Jeon, H.-D.Kim Jung, D.K. Lim, H. Lee, S. Kim, Bond character of thiophene on Ge(100): effects of coverage and temperature, J. Phys. Chem. B 110 (2006) 21728–21734, https://doi.org/10.1021/jp064251r.

[25] H. Zhu, W. Guo, M. Li, L. Zhao, S. Li, Y. Li, X. Lu, H. Shan, Density functional theory study of the adsorption and desulfurization of thiophene and its hydrogenated derivatives on Pt(111): implication for the mechanism of hydrodesulfurization over noble metal catalysts, ACS. Catal. 1 (2011) 1498–1510, https://doi.org/10.1021/cs2002548.

[26] L. Wang, L. Zhao, C. Xu, Y. Wang, J. Gao, Screening of active metals for reactive adsorption desulfurization adsorbent using density functional theory, Appl. Surf. Sci. 399 (2017) 440–450, https://doi.org/10.1016/j.apsusc.2016.11.160.

[27] J. Park, H.-K. Lee, A. Soon, B.D. Yu, S. Hong, Thermally induced desulfurization: structural transformation of thiophene on the Si(100) surface, J. Phys. Chem. C 117 (2013) 11731–11737, https://doi.org/10.1021/jp306495k.

[28] X. Lu, X. Xu, N. Wang, Q. Zhang, M.C. Lin, Chemisorption and decomposition of thiophene and Furan on the Si(100)-2 × 1 Surface: a quantum chemical study, J. Phys. Chem. B 105 (2001) 10069–10075, https://doi.org/10.1021/jp012254s.

[29] L.L. Cai, Y.L. Tian, X.B. Yuan, G.C. Hu, J.F. Ren, Spin polarization properties at the spinterface of thiophene/Fe(100): first principles calculations, Int. J. Mod. Phys. B 31 (2017) 1750072, https://doi.org/10.1142/S0217979217500722.

[30] G. Liu, J.A. Rodriguez, J. Dvorak, J. Hrbek, T. Jirsak, Chemistry of sulfur-containing molecules on Au(111): thiophene, sulfur dioxide, and methanethiol adsorption, Surf. Sci. 505 (2002) 295–307, https://doi.org/10.1016/S0039-6028(02)01377-8.

[31] M. Callsen, N. Atodiresei, V. Caciuc, S. Blügel, Semiempirical van der Waals interactions versus *ab initio* nonlocal correlation effects in the thiophene-Cu(111) system, Phys. Rev. B 86 (2012) 085439, https://doi.org/10.1103/PhysRevB.86.085439.

[32] Z.-X. Hu, H. Lan, W. Ji, Role of the dispersion force in modeling the interfacial properties of molecule-metal interfaces: adsorption of thiophene on copper surfaces, Sci. Rep. 4 (2014) 5036, https://doi.org/10.1038/srep05036.

[33] N. Isobe, T. Shibayama, Y. Mori, K. Shobatake, K. Sawabe, Adsorption structures of thiophene on Si(1 0 0)-(2 × 1) studied by scanning tunneling microscopy and density functional theory, Chem. Phys. Lett. 443 (2007) 347–351, https://doi.org/10.1016/j.cplett.2007.06.101.

[34] L. Buimaga-Iarinca, C. Morari, Adsorption of small aromatic molecules on gold: a DFT localized basis set study including van der Waals effects, Theor. Chem. Acc. 133 (2014) 1502, https://doi.org/10.1007/s00214-014-1502-9.

[35] F. Elfeninat, C. Fredriksson, E. Sacher, A. Selmani, A theoretical investigation of the interactions between thiophene and vanadium, chromium, copper, and gold, J. Chem. Phys. 102 (1995) 6153–6158, https://doi.org/10.1063/1.469349.

[36] K. Tonigold, A. Groß, Adsorption of small aromatic molecules on the (111) surfaces of noble metals: a density functional theory study with semiempirical corrections for dispersion effects, J. Chem. Phys. 132 (2010) 224701, https://doi.org/10.1063/1.3439691.

[37] H. Zhu, X. Li, N. Shi, X. Ding, Z. Yu, W. Zhao, H. Ren, Y. Pan, Y. Liu, W. Guo, Density functional theory study of thiophene desulfurization and conversion of desulfurization products on the Ni(111) surface and Ni_{55} cluster: implication for the mechanism of reactive adsorption desulfurization over Ni/ZnO catalysts, Catal. Sci. Technol. 11 (2021) 1615–1625, https://doi.org/10.1039/D0CY01523G.

[38] F. Mittendorfer, Initial steps in the desulfurization of thiophene/Ni(100)—A DFT study, J. Catal. 214 (2003) 234–241, https://doi.org/10.1016/S0021-9517(02)00149-5.

[39] W. Malone, H. Yildirim, J. Matos, A. Kara, A van der Waals inclusive density functional theory study of the nature of bonding for thiophene adsorption on Ni (100) and Cu(100) surfaces, J. Phys. Chem. C 121 (2017) 6090–6103, https://doi.org/10.1021/acs.jpcc.6b12064.

[40] J. Stöhr, E.B. Kollin, D.A. Fischer, J.B. Hastings, F. Zaera, F. Sette, Surface extended X-ray-absorption fine structure of low- Z adsorbates studied with fluorescence detection, Phys. Rev. Lett. 55 (1985) 1468–1471, https://doi.org/10.1103/PhysRevLett.55.1468.

[41] F. Zaera, E.B. Kollin, J.L. Gland, Thiophene chemisorption and thermal decomposition on nickel(100) single-crystal surfaces, Langmuir. 3 (1987) 555–557, https://doi.org/10.1021/la00076a020.

[42] W. Malone, W. Kaden, A. Kara, Exploring thiophene desulfurization: the adsorption of thiophene on transition metal surfaces, Surf. Sci. 686 (2019) 30–38, https://doi.org/10.1016/j.susc.2019.03.009.

[43] W. Malone, W.E. Kaden, A. Kara, Using DFT models of thiophene adsorption at transition metal interfaces to interpret periodic trends in thiophene hydrodesulfurization on transition metal sulfides, Catal. Lett. 149 (2019) 2953–2960, https://doi.org/10.1007/s10562-019-02864-x.

[44] M. Andersen, S.V. Levchenko, M. Scheffler, K. Reuter, Beyond scaling relations for the description of catalytic materials, ACS. Catal. 9 (2019) 2752–2759, https://doi.org/10.1021/acscatal.8b04478.

[45] L.M. Ghiringhelli, J. Vybiral, S.V. Levchenko, C. Draxl, M. Scheffler, Big data of materials science: critical role of the descriptor, Phys. Rev. Lett. 114 (2015) 105503, https://doi.org/10.1103/PhysRevLett.114.105503.

[46] A. Mazheika, Y.-G. Wang, R. Valero, F. Viñes, F. Illas, L.M. Ghiringhelli, S.V. Levchenko, M. Scheffler, Artificial-intelligence-driven discovery of catalyst genes with application to CO2 activation on semiconductor oxides, Nat. Commun. 13 (2022) 419, https://doi.org/10.1038/s41467-022-28042-z.

[47] O. Mamun, K.T. Winther, J.R. Boes, T. Bligaard, A Bayesian framework for adsorption energy prediction on bimetallic alloy catalysts, NPJ. Comput. Mater. 6 (2020) 177, https://doi.org/10.1038/s41524-020-00447-8.

[48] X. Ma, Z. Li, L.E.K. Achenie, H. Xin, Machine-learning-augmented chemisorption model for CO_2 electroreduction catalyst screening, J. Phys. Chem. Lett. 6 (2015) 3528–3533, https://doi.org/10.1021/acs.jpclett.5b01660.

[49] Z.W. Ulissi, M.T. Tang, J. Xiao, X. Liu, D.A. Torelli, M. Karamad, K. Cummins, C. Hahn, N.S. Lewis, T.F. Jaramillo, K. Chan, J.K. Nørskov, Machine-learning methods enable exhaustive searches for active bimetallic facets and reveal active site motifs for CO_2 reduction, ACS. Catal. 7 (2017) 6600–6608, https://doi.org/10.1021/acscatal.7b01648.

[50] S. Back, J. Yoon, N. Tian, W. Zhong, K. Tran, Z.W. Ulissi, Convolutional neural network of atomic surface structures to predict binding energies for high-throughput screening of catalysts, J. Phys. Chem. Lett. 10 (2019) 4401–4408, https://doi.org/10.1021/acs.jpclett.9b01428.

[51] K.T. Winther, M.J. Hoffmann, J.R. Boes, O. Mamun, M. Bajdich, T. Bligaard, Catalysis-Hub.org, an open electronic structure database for surface reactions, Sci. Data 6 (2019) 75, https://doi.org/10.1038/s41597-019-0081-y.

[52] A. Jain, S.P. Ong, G. Hautier, W. Chen, W.D. Richards, S. Dacek, S. Cholia, D. Gunter, D. Skinner, G. Ceder, K.A. Persson, Commentary: the materials project: a materials genome approach to accelerating materials innovation, APL Mater. 1 (2013) 011002, https://doi.org/10.1063/1.4812323.

[53] D.D. Landis, J.S. Hummelshoj, S. Nestorov, J. Greeley, M. Dulak, T. Bligaard, J.K. Norskov, K.W. Jacobsen, The computational materials repository, Comput. Sci. Eng. 14 (2012) 51–57, https://doi.org/10.1109/MCSE.2012.16.

[54] S. Kirklin, J.E. Saal, B. Meredig, A. Thompson, J.W. Doak, M. Aykol, S. Rühl, C. Wolverton, The Open Quantum Materials Database (OQMD): assessing the accuracy of DFT formation energies, NPJ. Comput. Mater. 1 (2015) 15010, https://doi.org/10.1038/npjcompumats.2015.10.

[55] R.O. Jones, Density functional theory: its origins, rise to prominence, and future, Rev. Mod. Phys. 87 (2015) 897–923, https://doi.org/10.1103/RevModPhys.87.897.

[56] P. Giannozzi, O. Andreussi, T. Brumme, O. Bunau, M. Buongiorno Nardelli, M. Calandra, R. Car, C. Cavazzoni, D. Ceresoli, M. Cococcioni, N. Colonna, I. Carnimeo, A. Dal Corso, S. De Gironcoli, P. Delugas, R.A. DiStasio, A. Ferretti, A. Floris, G. Fratesi, G. Fugallo, R. Gebauer, U. Gerstmann, F. Giustino, T. Gorni, J. Jia, M. Kawamura, H.-Y. Ko, A. Kokalj, E. Küçükbenli, M. Lazzeri, M. Marsili, N. Marzari, F. Mauri, N.L. Nguyen, H.-V. Nguyen, A. Otero-de-la-Roza, L. Paulatto, S. Poncé, D. Rocca, R. Sabatini, B. Santra, M. Schlipf, A.P. Seitsonen, A. Smogunov, I. Timrov, T. Thonhauser, P. Umari, N. Vast, X. Wu, S. Baroni, Advanced capabilities for materials modelling with Quantum ESPRESSO, J. Phys.: Condens. Matter 29 (2017) 465901, https://doi.org/10.1088/1361-648X/aa8f79.

[57] P. Giannozzi, S. Baroni, N. Bonini, M. Calandra, R. Car, C. Cavazzoni, D. Ceresoli, G.L. Chiarotti, M. Cococcioni, I. Dabo, A. Dal Corso, S. De Gironcoli, S. Fabris, G. Fratesi, R. Gebauer, U. Gerstmann, C. Gougoussis, A. Kokalj, M. Lazzeri, L. Martin-Samos, N. Marzari, F. Mauri, R. Mazzarello, S. Paolini, A. Pasquarello, L. Paulatto, C. Sbraccia, S. Scandolo, G. Sclauzero, A.P. Seitsonen, A. Smogunov, P. Umari, R.M. Wentzcovitch, QUANTUM ESPRESSO: a modular and open-source software project for quantum simulations of materials, J. Phys.: Condens. Matter 21 (2009) 395502, https://doi.org/10.1088/0953-8984/21/39/395502.

[58] J. Wellendorff, K.T. Lundgaard, A. Møgelhøj, V. Petzold, D.D. Landis, J.K. Nørskov, T. Bligaard, K.W. Jacobsen, Density functionals for surface science: Exchange-correlation model development with Bayesian error estimation, Phys. Rev. B 85 (2012) 235149. https://doi.org/10.1103/PhysRevB.85.235149.

[59] J.P. Perdew, J.A. Chevary, S.H. Vosko, K.A. Jackson, M.R. Pederson, D.J. Singh, C. Fiolhais, Atoms, molecules, solids, and surfaces: applications of the generalized gradient approximation for exchange and correlation, Phys. Rev. B 46 (1992) 6671–6687, https://doi.org/10.1103/PhysRevB.46.6671.

[60] D.C. Langreth, M.J. Mehl, Beyond the local-density approximation in calculations of ground-state electronic properties, Phys. Rev. B 28 (1983) 1809–1834, https://doi.org/10.1103/PhysRevB.28.1809.

[61] A.D. Becke, Density-functional exchange-energy approximation with correct asymptotic behavior, Phys. Rev. A 38 (1988) 3098–3100, https://doi.org/10.1103/PhysRevA.38.3098.

[62] A. Tkatchenko, L. Romaner, O.T. Hofmann, E. Zojer, C. Ambrosch-Draxl, M. Scheffler, Van der Waals interactions between organic adsorbates and at organic/inorganic interfaces, MRS Bull 35 (2010) 435–442, https://doi.org/10.1557/mrs2010.581.

[63] J. Klimeš, D.R. Bowler, A. Michaelides, Van der Waals density functionals applied to solids, Phys. Rev. B 83 (2011) 195131, https://doi.org/10.1103/PhysRevB.83.195131.

[64] J. Carrasco, B. Santra, J. Klimeš, A. Michaelides, To wet or not to wet? Dispersion forces tip the balance for water ice on metals, Phys. Rev. Lett. 106 (2011) 026101, https://doi.org/10.1103/PhysRevLett.106.026101.

[65] J. Carrasco, J. Klimeš, A. Michaelides, The role of van der Waals forces in water adsorption on metals, J. Chem. Phys. 138 (2013) 024708, https://doi.org/10.1063/1.4773901.

[66] J. Klimeš, A. Michaelides, Perspective: advances and challenges in treating van der Waals dispersion forces in density functional theory, J. Chem. Phys. 137 (2012) 120901, https://doi.org/10.1063/1.4754130.

[67] W. Malone, A. Kara, Chemisorption characteristics of pyridine on Rh, Pd, Pt and Ni(1 1 1), Electron. Struct. 2 (2020) 015001, https://doi.org/10.1088/2516-1075/ab6aab.

[68] W. Liu, J. Carrasco, B. Santra, A. Michaelides, M. Scheffler, A. Tkatchenko, Benzene adsorbed on metals: concerted effect of covalency and van der Waals bonding, Phys. Rev. B 86 (2012) 245405, https://doi.org/10.1103/PhysRevB.86.245405.

[69] G. Henkelman, A. Arnaldsson, H. Jónsson, A fast and robust algorithm for Bader decomposition of charge density, Comput. Mater. Sci. 36 (2006) 354–360, https://doi.org/10.1016/j.commatsci.2005.04.010.

[70] M. Yu, D.R. Trinkle, Accurate and efficient algorithm for Bader charge integration, J. Chem. Phys. 134 (2011) 064111, https://doi.org/10.1063/1.3553716.

[71] W. Tang, E. Sanville, G. Henkelman, A grid-based Bader analysis algorithm without lattice bias, J. Phys.: Condens. Matter 21 (2009) 084204, https://doi.org/10.1088/0953-8984/21/8/084204.

[72] E. Sanville, S.D. Kenny, R. Smith, G. Henkelman, Improved grid-based algorithm for Bader charge allocation, J. Comput. Chem. 28 (2007) 899–908, https://doi.org/10.1002/jcc.20575.

[73] O. Mamun, K.T. Winther, J.R. Boes, T. Bligaard, High-throughput calculations of catalytic properties of bimetallic alloy surfaces, Sci. Data 6 (2019) 76, https://doi.org/10.1038/s41597-019-0080-z.

[74] G. Kresse, J. Furthmüller, Efficiency of ab-initio total energy calculations for metals and semiconductors using a plane-wave basis set, Comput. Mater. Sci. 6 (1996) 15–50, https://doi.org/10.1016/0927-0256(96)00008-0.
[75] G. Kresse, J. Furthmüller, Efficient iterative schemes for *ab initio* total-energy calculations using a plane-wave basis set, Phys. Rev. B 54 (1996) 11169–11186, https://doi.org/10.1103/PhysRevB.54.11169.
[76] J.F. Annett, Efficiency of algorithms for Kohn-Sham density functional theory, Comput. Mater. Sci. 4 (1995) 23–42, https://doi.org/10.1016/0927-0256(94)00013-3.
[77] Y. Zhou, H. Wang, Y. Liu, X. Gao, H. Song, Applicability of Kerker preconditioning scheme to the self-consistent density functional theory calculations of inhomogeneous systems, Phys. Rev. E 97 (2018) 033305, https://doi.org/10.1103/PhysRevE.97.033305.
[78] L.D. Marks, D.R. Luke, Robust mixing for *ab initio* quantum mechanical calculations, Phys. Rev. B 78 (2008) 075114, https://doi.org/10.1103/PhysRevB.78.075114.
[79] T.J. Boerner, S. Deems, T.R. Furlani, S.L. Knuth, J. Towns, ACCESS: advancing innovation: nSF's advanced cyberinfrastructure coordination ecosystem: services & support. Practice and Experience in Advanced Research Computing, ACM, Portland OR USA, 2023, pp. 173–176, https://doi.org/10.1145/3569951.3597559.